



## MICCAI 2008 Workshop Proceedings

### Computational Biomechanics for Medicine III

Karol Miller, Poul M.F. Nielsen

<http://www.mech.uwa.edu.au/CBM2008>





## **Preface:**

A novel partnership between surgeons and machines, made possible by advances in computing and engineering technology, could overcome many of the limitations of traditional surgery. By extending surgeons' ability to plan and carry out surgical interventions more accurately and with less trauma, Computer-Integrated Surgery (CIS) systems could help to improve clinical outcomes and the efficiency of health care delivery. CIS systems could have a similar impact on surgery to that long since realized in Computer-Integrated Manufacturing (CIM). Mathematical modeling and computer simulation have proved tremendously successful in engineering. Computational mechanics has enabled technological developments in virtually every area of our lives. One of the greatest challenges for mechanists is to extend the success of computational mechanics to fields outside traditional engineering, in particular to biology, the biomedical sciences, and medicine.

Computational Biomechanics for Medicine Workshop series was established in 2006 with the first meeting held in Copenhagen. The third workshop was held in conjunction with the Medical Image Computing and Computer Assisted Intervention Conference (MICCAI 2008) in New York on 10 September 2008. It provided an opportunity for specialists in computational sciences to present and exchange opinions on the possibilities of applying their techniques to computer-integrated medicine.

Computational Biomechanics for Medicine III was organized into two streams: Computational Biomechanics of Soft Tissues, and Computational Biomechanics of Tissues of Musculoskeletal System. The application of advanced computational methods to the following areas was discussed:

- Medical image analysis;
- Image-guided surgery;
- Surgical simulation;
- Surgical intervention planning;
- Disease prognosis and diagnosis;
- Injury mechanism analysis;
- Implant and prostheses design;
- Medical robotics.

After rigorous review of full (eight-to-twelve page) manuscripts we accepted 15 papers, collected in this volume. They were split equally between podium and poster presentations. The proceedings also include abstracts of two invited lectures by world-leading researchers Professor Chwee Teck Lim from national University of Singapore and Dr. David Lloyd from The University of Western Australia.

Information about Computational Biomechanics for Medicine Workshops, including Proceedings of previous meetings is available at <http://cbm.mech.uwa.edu.au/> .

We would like to thank the MICCAI 2008 organizers for help with administering the Workshop, invited lecturers for deep insights into their research fields, the authors for submitting high quality work, and the reviewers for helping with paper selection.

**Karol Miller**  
**Poul M.F. Nielsen**

## Contents:

### Invited Lectures

1. Molecular and Cellular Biomechanics-based Insights into the Pathophysiology of Human Diseases  
*Chwee Teck Lim* 2
2. Computation Biomechanics: Neuromuscular skeletal modelling to estimate tissue loading in the lower limbs  
*David Lloyd* 3

### Part 1. Computational Biomechanics Of Soft Tissues

3. Cardiac motion estimation using multi-scale feature points  
*Becciu A; van Assen H; Florack L; Janssen B; ter Haar Romeny B* 5
4. Fast image-based model of mitral valve closure for surgical planning  
*Hammer P; Vasilyev N; Perrin D; del Nido P; Howe R* 15
5. Multimodal Registration of White Matter Brain Data via Optimal Mass Transport  
*Rehman, Tauseef; Haber, Eldad; Pohl, Kilian; Haker, Steven; Halle, Mike; Talos, Florin; Wald, Lawrence; Kikinis, Ron; Tannenbaum, Allen* 27
6. Cardiac Motion Recovery by Coupling an Electromechanical Model and Cine-MRI Data: First Steps  
*Billet F; Sermesant M; Delingette H; Ayache N* 36
7. Inverse Nonlinear Finite Element Methods for Surgery Simulation and Image Guidance  
*Pratt P* 48
8. Nonlinear Elastic Registration with Unbiased Regularization in Three Dimensions  
*Yanovsky I; Le Guyader C; Leow A; Thompson P; Vese L* 56
9. Coupling Finite Element and Mesh-free Methods for Modelling Brain Deformation in Response to Tumour Growth  
*Berger, Jamie; Horton, Asley; Joldes, Grand; Wittek, Adam; Miller, Karol* 68

10.	Simulation of Active Cardiac Dynamics with Orthotropic Hyperelastic Material Model <i>Wong, Ken C.L.; Wang, Linwei; Zhang, Heye; Liu, Huafeng; Shi, Pengcheng</i>	83
11.	Realistic And Efficient Brain-Skull Interaction Model For Brain Shift Computation <i>Joldes, Grand Roman; Wittek, Adam; Miller, Karol; Morriss, Leith</i>	95
12.	Integration of Geometrical Boundary Conditions on Soft Tissue Characterization under large deformation <i>Ahn B; Kim J</i>	106
13.	Finite Element Modeling of the Pulse Wave propagation in the aorta for simulation of the Pulse Wave Imaging (PWI) method <i>Jonathan Vappou; Ioannis Zervantonakis; Jianwen Luo; Elisa Konofagou</i>	118
14.	Comparison of Displacement-Based and Force-Based Mapped Meshing <i>Vincent A. Magnotta; Wen Li; Nicole M. Grosland</i>	128

## **Part 2. Computational Biomechanics Of Tissues Of Musculoskeletal System**

15.	Assessment of Peri-Articular Implant Fitting Based on Statistical Finite Element Modeling <i>Bonaretti S; Reimers N; Reyes M; Nikitsin A; Joensson A; Nolte L</i>	138
16.	Orientation definition of anisotropy is important to finite element simulation of bone material properties <i>Yang H; Guo T; Ma X</i>	148
17.	A Mix-resolution Bone-related Statistical Deformable Model (mBr-SDM) for Soft Tissue Prediction in Orthognathic Surgery Planning <i>He Q; Ip H; Xia J</i>	159

# Nonlinear Elastic Registration with Unbiased Regularization in Three Dimensions

Igor Yanovsky<sup>1</sup>, Carole Le Guyader<sup>2</sup>, Alex Leow<sup>3</sup>,  
Paul Thompson<sup>3</sup> and Luminita Vese<sup>1</sup>

August 1, 2008

<sup>1</sup>Department of Mathematics, University of California, Los Angeles, CA, USA

<sup>2</sup>Institute of Mathematical Research of Rennes, France

<sup>3</sup>Laboratory of Neuro Imaging, UCLA School of Medicine, Los Angeles, CA, USA

## Abstract

We propose a new nonlinear image registration model which is based on nonlinear elastic regularization and unbiased registration. The nonlinear elastic and the unbiased regularization terms are simplified using the change of variables by introducing an unknown that approximates the Jacobian matrix of the displacement field. This reduces the minimization to involve linear differential equations. In contrast to recently proposed unbiased fluid registration method, the new model is written in a unified variational form and is minimized using gradient descent. As a result, the new unbiased nonlinear elasticity model is computationally more efficient and easier to implement than the unbiased fluid registration. The unbiased large-deformation nonlinear elasticity method was tested using volumetric serial magnetic resonance images and shown to have some advantages for medical imaging applications.

## 1 Introduction

Given two images, the source and target, the goal of image registration is to find an optimal diffeomorphic spatial transformation such that the deformed source image is aligned with the target image. In the case of non-parametric registration methods (the class of methods we are interested in), the problem can be phrased as a functional minimization problem whose unknown is the displacement vector field  $\mathbf{u}$ . Usually, the devised functional consists of a distance measure (intensity-based, correlation-based, mutual-information based [11] or metric-structure-comparison based [10]) and a regularizer that guarantees smoothness of the displacement vector field. Several regularizers have been investigated (see Part II of [11] for a review). Generally, physical arguments motivate the selection of the regularizer. Among those currently used is the linear elasticity smoother first introduced by Broit [2]. The objects to be registered are considered to be observations of the same elastic body at two different times, before and after being subjected to a deformation as mentioned in [11]. The smoother, in this case, is the linearized elastic potential of the displacement vector field. However, this model is unsuitable for problems involving large-magnitude deformations.

In [5], Christensen *et al.* proposed a viscous fluid model to overcome this issue. Given the force field  $\mathbf{f}$ , the deforming image is considered to be embedded in viscous fluid whose motion is governed by Navier-Stokes equations for conservation of momentum:

$$\mu\Delta\mathbf{v}(\mathbf{x},t) + (\nu + \mu)\nabla(\nabla \cdot \mathbf{v}(\mathbf{x},t)) = \mathbf{f}(\mathbf{x},\mathbf{u}(\mathbf{x},t)), \quad (1)$$

$$\mathbf{v}(\mathbf{x},t) = \mathbf{u}_t(\mathbf{x},t) + \nabla\mathbf{u}(\mathbf{x},t) \cdot \mathbf{v}(\mathbf{x},t). \quad (2)$$

Here, equation (2), defining material derivative of the displacement field  $\mathbf{u}$ , nonlinearly relates the velocity  $\mathbf{v}$  and displacement vector fields. Constants  $\mu$  and  $\nu$  are viscosity coefficients of a fluid.

One drawback of this method is the computational cost. Numerically, the image-derived force field  $\mathbf{f}(\mathbf{x},\mathbf{u}(\mathbf{x},t))$  is first computed at time  $t$ . Fixing the force field  $\mathbf{f}$ , linear equation (1) is solved for  $\mathbf{v}(\mathbf{x},t)$  numerically using the successive over-relaxation (SOR) scheme. Then, an explicit Euler scheme is used to advance  $\mathbf{u}$  in time. Recent works [3, 14, 13] applied Riemannian nonlinear elasticity priors to deformation velocity fields. These alternating frameworks, however, are time-consuming, which motivates the search for faster implementations (see for instance [1] or [7] in which the instantaneous velocity  $\mathbf{v}$  is obtained by convolving  $\mathbf{f}$  with a Gaussian kernel).

In this paper, we propose an alternative approach to fluid registration. The proposed model is derived from a variational problem which is not in the form of a two-step algorithm and which can produce large-magnitude deformations. For that purpose, a nonlinear elasticity smoother is introduced. As will be seen later, the computation of the Euler-Lagrange equations in this case is cumbersome. We circumvent this issue by introducing a second unknown, a matrix variable  $V$ , which approximates the Jacobian matrix of  $\mathbf{u}$ . The nonlinear elastic regularizer is now applied to  $V$ . The Euler-Lagrange equations are straightforwardly derived and a gradient descent method is used.

Also, allowing large deformations to occur may yield non-diffeomorphic deformation mappings (at least at the discrete level). In [5], Christensen *et al.* proposed a regriding technique that resamples the deforming image and re-initializes the process once the value of the deformation Jacobian drops below a certain threshold. In [8], Haber and Modersitzki introduced an elastic registration model subject to volume-preserving constraints. To ensure that the transformation  $\mathbf{g}(\mathbf{x}) = \mathbf{x} - \mathbf{u}(\mathbf{x})$  is volume-preserving (that is, for any domain  $\Omega$ ,  $\int_{\Omega} d\mathbf{x} = \int_{\mathbf{g}(\Omega)} d\mathbf{x}$ ), they proposed the following pointwise constraint:  $\det(I - D\mathbf{u}(\mathbf{x})) - 1 = 0$ . Pursuing the same direction in [9], the authors introduced a minimization problem under inequality constraints on the Jacobian.

Here we use an information-theoretic approach previously introduced in [16]. In [16], the authors considered

a smooth deformation  $\mathbf{g}$  that maps domain  $\Omega$  bijectively onto itself. Consequently,  $\mathbf{g}$  and  $\mathbf{g}^{-1}$  are bijective and globally volume-preserving. Probability density functions can thus be associated with the deformation  $\mathbf{g}$  and its inverse  $\mathbf{g}^{-1}$ . The authors then proposed to quantify the magnitude of the deformation by means of the symmetric Kullback-Leibler distance between the probability density functions associated with the deformation and the identity mapping. This distance, when rewritten using skew-symmetry properties, is viewed as a cost function and is combined with the viscous fluid model for registration, which leads to an unbiased fluid registration model. Unlike the unbiased fluid registration model, the unbiased nonlinear elasticity method, introduced here, allows the functional to be written “in closed form”. The new model also does not require expensive Navier-Stokes solver (or its approximation) at each step as previously mentioned.

## 2 Method

Let  $\Omega$  be an open and bounded domain in  $\mathbb{R}^3$ . Without loss of generality, we assume that the volume of  $\Omega$  is 1, i.e.  $|\Omega| = 1$ . Let  $I_1, I_2 : \Omega \rightarrow \mathbb{R}$  be the two volumetric images to be registered. We seek the transformation  $\mathbf{g} : \Omega \rightarrow \Omega$  that maps the source image  $I_2$  into correspondence with the target image  $I_1$ . In this paper, we will restrict this mapping to be differentiable, one-to-one, and onto. We denote the Jacobian matrix of a deformation  $\mathbf{g}$  to be  $D\mathbf{g}$ , with Jacobian denoted by  $|D\mathbf{g}(\mathbf{x})| = \det(D\mathbf{g}(\mathbf{x}))$  (thus we will use the notation  $|V| := \det(V)$  for any  $3 \times 3$  matrix  $V$ ). The displacement field  $\mathbf{u}(\mathbf{x})$  from the position  $\mathbf{x}$  in the deformed image  $I_2 \circ \mathbf{g}(\mathbf{x})$  back to  $I_2(\mathbf{x})$  is defined in terms of the deformation  $\mathbf{g}(\mathbf{x})$  by the expression  $\mathbf{g}(\mathbf{x}) = \mathbf{x} - \mathbf{u}(\mathbf{x})$  at every point  $\mathbf{x} \in \Omega$ . Thus, we consider the problems of finding  $\mathbf{g}$  and  $\mathbf{u}$  as equivalent.

In general, nonlinear image registration models may be formulated in a variational framework. The minimization problems often define the energy functional  $E$  as a linear combination of an image matching term  $F$  and a regularizing term  $R$ :  $\inf_{\mathbf{u}} \{E(\mathbf{u}) = F(\mathbf{u}) + \lambda_0 R(\mathbf{u})\}$ . Here,  $\lambda_0 > 0$  is a weighting parameter.

### 2.1 Registration metrics

In this paper, the matching functional  $F$  takes the form of the  $L^2$  norm (the sum of squared intensity differences),  $F = F_{L^2}$ , and the mutual information,  $F = F_{MI}$ .

**$L^2$ -norm:** The  $L^2$ -norm matching functional is suitable when the images have been acquired through similar sensors (with additive Gaussian noise) and thus are expected to present the same intensity range and distribution. The  $L^2$  distance between the deformed image  $I_2 \circ \mathbf{g}(\mathbf{x}) = I_2(\mathbf{x} - \mathbf{u}(\mathbf{x}))$  and target image  $I_1(\mathbf{x})$  is defined as

$$F_{L^2}(\mathbf{u}) = \frac{1}{2} \int_{\Omega} (I_2(\mathbf{x} - \mathbf{u}(\mathbf{x})) - I_1(\mathbf{x}))^2 d\mathbf{x}. \quad (3)$$

**Mutual Information:** Mutual information can be used to align images of different modalities, without requiring knowledge of the relationship of the two registered images [6, 15]. Here, the intensity distributions estimated from  $I_1(\mathbf{x})$  and  $I_2(\mathbf{x} - \mathbf{u}(\mathbf{x}))$  are denoted by  $p^{I_1}$  and  $p_{\mathbf{u}}^{I_2}$ , respectively, and an estimate of their joint intensity distribution by  $p_{\mathbf{u}}^{I_1, I_2}$ . We let  $i_1 = I_1(\mathbf{x})$ ,  $i_2 = I_2(\mathbf{x} - \mathbf{u}(\mathbf{x}))$  denote intensity values at point  $\mathbf{x} \in \Omega$ . Given the displacement field  $\mathbf{u}$ , the mutual information computed from  $I_1$  and  $I_2$  is provided by

$$MI_{\mathbf{u}}^{I_1, I_2} = \int_{\mathbb{R}^2} p_{\mathbf{u}}^{I_1, I_2}(i_1, i_2) \log[p_{\mathbf{u}}^{I_1, I_2}(i_1, i_2) / (p^{I_1}(i_1) p_{\mathbf{u}}^{I_2}(i_2))] di_1 di_2.$$

We seek to maximize the mutual information between  $I_2(\mathbf{x} - \mathbf{u}(\mathbf{x}))$  and  $I_1(\mathbf{x})$ , or equivalently, minimize the negative of  $MI_{\mathbf{u}}^{I_1, I_2}$ :

$$F_{MI}(I_1, I_2, \mathbf{u}) = -MI_{\mathbf{u}}^{I_1, I_2}. \quad (4)$$



## 2.2 Nonlinear Elastic Regularization

The theory of elasticity is based on the notion of strain. Strain is defined as the amount of deformation an object experiences compared to its original size and shape. In three spatial dimensions, the strain tensor,  $\mathcal{E} = [\varepsilon_{ij}] \in \mathbb{R}^{3 \times 3}$ ,  $1 \leq i, j \leq 3$ , is a symmetric tensor used to quantify the strain of an object undergoing a deformation. The nonlinear strain is defined as

$$\varepsilon_{ij}(\mathbf{u}) = \frac{1}{2}(\partial_j u_i + \partial_i u_j + \sum_{k=1}^3 \partial_i u_k \partial_j u_k),$$

with the nonlinear strain tensor matrix given by

$$\mathcal{E}(\mathbf{u}) = \frac{1}{2}(D\mathbf{u}^t + D\mathbf{u} + D\mathbf{u}^t D\mathbf{u}). \quad (5)$$

Stored energy (Saint Venant-Kirchhoff material) is defined as

$$W(\mathcal{E}) = \frac{\nu}{2}(\text{trace}(\mathcal{E}))^2 + \mu \text{trace}(\mathcal{E}^2),$$

where  $\nu$  and  $\mu$  are Lamé elastic material constants. The regularization for nonlinear elasticity becomes

$$R_E(\mathbf{u}) = \int_{\Omega} W(\mathcal{E}(\mathbf{u})) d\mathbf{x}.$$

The regularization term  $R_E(\mathbf{u})$  can be minimized with respect to  $\mathbf{u}$ . However, since the regularization term is written in terms of partial derivatives of components of  $\mathbf{u}$ , the Euler-Lagrange equations become complicated and are computationally expensive to minimize. Instead, following earlier theoretical work [12], we minimize an approximate functional by introducing the matrix variable

$$V \approx D\mathbf{u} \quad (6)$$

and thus consider a new form of nonlinear elasticity regularization functional

$$R_E(\mathbf{u}, V) = \int_{\Omega} W(\widehat{V}) d\mathbf{x} + \frac{\beta}{2} \int_{\Omega} \|V - D\mathbf{u}\|_F^2 d\mathbf{x}, \quad (7)$$

where  $\widehat{V} = \frac{1}{2}(V^t + V + V^t V)$ ,  $\beta$  is a positive constant, and  $\|\cdot\|_F$  denotes the Frobenius norm. In the limit, as  $\beta \rightarrow +\infty$ , we obtain  $V \approx D\mathbf{u}$  in the  $L^2$  topology.

## 2.3 Unbiased Registration Constraint

In [16], the authors proposed an unbiased fluid image registration approach. In this context, *unbiased* means that the Jacobian determinants of the deformations recovered between a pair of images follow a log-normal distribution, with zero mean after log-transformation. The authors argued that this distribution is beneficial when recovering changes in regions of homogeneous intensity, and in ensuring symmetrical results when the order of two images being registered is switched. As derived in [16] using information theory, the unbiased regularization term is given as

$$R_{UB}(\mathbf{u}) = \int_{\Omega} (|D(\mathbf{x} - \mathbf{u}(\mathbf{x}))| - 1) \log |D(\mathbf{x} - \mathbf{u}(\mathbf{x}))| d\mathbf{x}. \quad (8)$$

It is important to note that  $R_{UB}$  generates inverse-consistent deformation maps. The inverse-consistent property of the unbiased technique was shown in a validation study of the unbiased fluid registration methods [17]. Also, to see why minimizing equation (8) leads to unbiased deformation in the logarithmic space, we observe that the integrand is always non-negative, and only evaluates to zero when the deformation  $\mathbf{g}$  is volume-preserving everywhere ( $|D\mathbf{g}| = 1$  everywhere). Thus, by treating it as a cost, we recover zero-change by minimizing this cost when we compare images differing only in noise.

Given equation (6), we have  $D\mathbf{g} = I - D\mathbf{u} \approx I - V$ , where  $I$  is the  $3 \times 3$  identity matrix. Therefore, as in subsection 2.2, to simplify the discretization, we introduce

$$R_{UB}(V) = \int_{\Omega} (|I - V| - 1) \log |I - V| d\mathbf{x}. \quad (9)$$

Recall that here  $|I - V| = \det(I - V)$ .

## 2.4 Unbiased Nonlinear Elasticity Registration

The total energy functional employed in this work, is given as a linear combination of the similarity measure  $F$  (which is either  $F_{L^2}$  from (3) or  $F_{MI}$  from (4)), nonlinear elastic regularization  $R_E$  in (7), and unbiased regularization  $R_{UB}$  in (9):

$$E(\mathbf{u}, V) = F(\mathbf{u}) + R_E(\mathbf{u}, V) + \lambda R_{UB}(V). \quad (10)$$

The explicit weighting parameter is omitted in front of  $R_E(\mathbf{u}, V)$ , since this term is weighted by Lamé constants  $\nu$  and  $\mu$ . We solve the Euler-Lagrange equations in  $\mathbf{u}$  and  $V$  using the gradient descent method, parameterizing the descent direction by an artificial time  $t$ ,

$$\frac{\partial \mathbf{u}}{\partial t} = -\partial_{\mathbf{u}} E(\mathbf{u}, V) = -\partial_{\mathbf{u}} F(\mathbf{u}) - \partial_{\mathbf{u}} R_E(\mathbf{u}, V), \quad (11)$$

$$\frac{\partial V}{\partial t} = -\partial_V E(\mathbf{u}, V) = -\partial_V R_E(\mathbf{u}, V) - \lambda \partial_V R_{UB}(V), \quad (12)$$

which gives systems of three and nine equations, respectively. Explicit expressions for the gradients and their discretizations are given in Section 3.

*Remark:* The regularization on the deformation  $\mathbf{g}$  proposed in this work can be expressed in a general form

$$R(\mathbf{g}) = \int_{\Omega} R_1(D\mathbf{g}) d\mathbf{x} + \int_{\Omega} R_2(|D\mathbf{g}|) d\mathbf{x},$$

with  $|D\mathbf{g}| := \det(D\mathbf{g})$ . For the minimization, an auxiliary variable can also be introduced to simplify the numerical calculations, removing the nonlinearity in the derivatives.

## 3 Implementation

### 3.1 The Energy Gradients

Computing the first variation of functional  $F_{L^2}$  in (3) gives the following gradient:  $\partial_{\mathbf{u}} F_{L^2}(\mathbf{u}) = -[I_2(\mathbf{x} - \mathbf{u}(\mathbf{x})) - I_1(\mathbf{x})] \nabla I_2(\mathbf{x} - \mathbf{u}(\mathbf{x}))$ .

The gradient of (4) is given by  $\partial_{\mathbf{u}} F_{MI}(\mathbf{u}) = (1/|\Omega|)[Q_{\mathbf{u}} * \partial G_{\sigma}/\partial \xi_2](I_1(\mathbf{x}), I_2(\mathbf{x} - \mathbf{u})) \nabla I_2(\mathbf{x} - \mathbf{u})$ , where  $Q_{\mathbf{u}}(i_1, i_2) = 1 + \log[p_{\mathbf{u}}^{I_1, I_2}(i_1, i_2)/p^{I_1}(i_1)p_{\mathbf{u}}^{I_2}(i_2)]$ , and  $G_{\sigma}(\xi_1, \xi_2)$  is a two-dimensional Gaussian kernel, with variance  $\sigma^2$ , which is used to estimate the joint intensity distribution from  $I_2(\mathbf{x} - \mathbf{u})$  and  $I_1(\mathbf{x})$ .

Computing the first variation of functional  $R_E(\mathbf{u}, V)$ , in equation (7), with respect to  $\mathbf{u}$  gives the following components of the gradient  $\partial_{\mathbf{u}} R_E(\mathbf{u}, V)$ :

$$\partial_{u_k} R_E(\mathbf{u}, V) = \beta(\partial_1 v_{k1} + \partial_2 v_{k2} + \partial_3 v_{k3} - \Delta u_k), \quad k = 1, 2, 3.$$

The first variation of  $R_E(\mathbf{u}, V)$  with respect to  $V$ , with  $V = [v_{ij}]$ , gives  $\partial_V R_E(\mathbf{u}, V)$ :

$$\begin{aligned} \partial_{v_{11}} R_E(\mathbf{u}, V) &= \beta(v_{11} - \partial_1 u_1) + \nu c_1(1 + v_{11}) + \mu(c_2(1 + v_{11}) + c_5 v_{12} + c_6 v_{13}), \\ \partial_{v_{12}} R_E(\mathbf{u}, V) &= \beta(v_{12} - \partial_2 u_1) + \nu c_1 v_{12} + \mu(c_3 v_{12} + c_5(1 + v_{11}) + c_7 v_{13}), \\ \partial_{v_{13}} R_E(\mathbf{u}, V) &= \beta(v_{13} - \partial_3 u_1) + \nu c_1 v_{13} + \mu(c_4 v_{13} + c_6(1 + v_{11}) + c_7 v_{12}), \\ \partial_{v_{21}} R_E(\mathbf{u}, V) &= \beta(v_{21} - \partial_1 u_2) + \nu c_1 v_{21} + \mu(c_2 v_{21} + c_5(1 + v_{22}) + c_6 v_{23}), \\ \partial_{v_{22}} R_E(\mathbf{u}, V) &= \beta(v_{22} - \partial_2 u_2) + \nu c_1(1 + v_{22}) + \mu(c_3(1 + v_{22}) + c_5 v_{21} + c_7 v_{23}), \\ \partial_{v_{23}} R_E(\mathbf{u}, V) &= \beta(v_{23} - \partial_3 u_2) + \nu c_1 v_{23} + \mu(c_4 v_{23} + c_6 v_{21} + c_7(1 + v_{22})), \\ \partial_{v_{31}} R_E(\mathbf{u}, V) &= \beta(v_{31} - \partial_1 u_3) + \nu c_1 v_{31} + \mu(c_2 v_{31} + c_5 v_{32} + c_6(1 + v_{33})), \\ \partial_{v_{32}} R_E(\mathbf{u}, V) &= \beta(v_{32} - \partial_2 u_3) + \nu c_1 v_{32} + \mu(c_3 v_{32} + c_5 v_{31} + c_7(1 + v_{33})), \\ \partial_{v_{33}} R_E(\mathbf{u}, V) &= \beta(v_{33} - \partial_3 u_3) + \nu c_1(1 + v_{33}) + \mu(c_4(1 + v_{33}) + c_6 v_{31} + c_7 v_{32}), \end{aligned}$$

where

$$\begin{aligned} c_1 &= v_{11} + v_{22} + v_{33} + \frac{1}{2}(v_{11}^2 + v_{21}^2 + v_{31}^2 + v_{12}^2 + v_{22}^2 + v_{32}^2 + v_{13}^2 + v_{23}^2 + v_{33}^2), \\ c_2 &= 2v_{11} + v_{11}^2 + v_{21}^2 + v_{31}^2, & c_5 &= v_{21} + v_{12} + v_{11}v_{12} + v_{21}v_{22} + v_{31}v_{32}, \\ c_3 &= 2v_{22} + v_{12}^2 + v_{22}^2 + v_{32}^2, & c_6 &= v_{31} + v_{13} + v_{11}v_{13} + v_{21}v_{23} + v_{31}v_{33}, \\ c_4 &= 2v_{33} + v_{13}^2 + v_{23}^2 + v_{33}^2, & c_7 &= v_{32} + v_{23} + v_{12}v_{13} + v_{22}v_{23} + v_{32}v_{33}. \end{aligned}$$

We can compute the first variation of (9), obtaining  $\partial_V R_{UB}(V)$ . We first simplify the notation, letting  $J = |I - V|$ . Also, denote  $L(J) = (J - 1) \log J$ . Hence,  $L'(J) = dL(J)/dJ = 1 + \log J - 1/J$ . Thus,

$$\begin{aligned} \partial_{v_{11}} R_{UB}(V) &= -((1 - v_{22})(1 - v_{33}) - v_{32}v_{23})L'(J), \\ \partial_{v_{12}} R_{UB}(V) &= -(v_{23}v_{31} + v_{21}(1 - v_{33}))L'(J), \\ \partial_{v_{13}} R_{UB}(V) &= -(v_{21}v_{32} + (1 - v_{22})v_{31})L'(J), \\ \partial_{v_{21}} R_{UB}(V) &= -(v_{32}v_{13} + v_{12}(1 - v_{33}))L'(J), \\ \partial_{v_{22}} R_{UB}(V) &= -((1 - v_{11})(1 - v_{33}) - v_{13}v_{31})L'(J), \\ \partial_{v_{23}} R_{UB}(V) &= -(v_{12}v_{31} + v_{32}(1 - v_{11}))L'(J), \\ \partial_{v_{31}} R_{UB}(V) &= -(v_{12}v_{23} + v_{13}(1 - v_{22}))L'(J), \\ \partial_{v_{32}} R_{UB}(V) &= -(v_{21}v_{13} + v_{23}(1 - v_{11}))L'(J), \\ \partial_{v_{33}} R_{UB}(V) &= -((1 - v_{11})(1 - v_{22}) - v_{12}v_{21})L'(J). \end{aligned}$$

### 3.2 Numerical Discretization

Let  $\Delta x_1, \Delta x_2, \Delta x_3$  be the spacial steps,  $\Delta t$  be the time step, and  $(x_{1i}, x_{2j}, x_{3k}) = (i\Delta x_1, j\Delta x_2, k\Delta x_3)$  be the grid points, for  $1 \leq i \leq M, 1 \leq j \leq N, 1 \leq k \leq P$ . For a function  $\varphi : \Omega \rightarrow \mathbb{R}$ , let  $\varphi_{i,j,k}^n =$

$\varphi(n\Delta t, i\Delta x_1, j\Delta x_2, k\Delta x_3)$ . We define the difference operators based on uniformly-spaced grid as

$$\begin{aligned} D^{x_1}\varphi_{i,j,k}^n &= \frac{\varphi_{i+1,j,k}^n - \varphi_{i-1,j,k}^n}{2\Delta x_1}, & D^{x_1x_1}\varphi_{i,j,k}^n &= \frac{\varphi_{i+1,j,k}^n - 2\varphi_{i,j,k}^n + \varphi_{i-1,j,k}^n}{\Delta x_1^2}, \\ D^{x_2}\varphi_{i,j,k}^n &= \frac{\varphi_{i,j+1,k}^n - \varphi_{i,j-1,k}^n}{2\Delta x_2}, & D^{x_2x_2}\varphi_{i,j,k}^n &= \frac{\varphi_{i,j+1,k}^n - 2\varphi_{i,j,k}^n + \varphi_{i,j-1,k}^n}{\Delta x_2^2}, \\ D^{x_3}\varphi_{i,j,k}^n &= \frac{\varphi_{i,j,k+1}^n - \varphi_{i,j,k-1}^n}{2\Delta x_3}, & D^{x_3x_3}\varphi_{i,j,k}^n &= \frac{\varphi_{i,j,k+1}^n - 2\varphi_{i,j,k}^n + \varphi_{i,j,k-1}^n}{\Delta x_3^2}. \end{aligned}$$

Below, we will use the following notations when it is obvious that the grid point at  $(i\Delta x_1, j\Delta x_2, k\Delta x_3)$  is under consideration:  $\varphi^n := \varphi_{i,j,k}^n$ ,  $D^{x_l}\varphi^n := D^{x_l}\varphi_{i,j,k}^n$ ,  $D^{x_lx_l}\varphi^n := D^{x_lx_l}\varphi_{i,j,k}^n$ ,  $l = 1, 2, 3$ .

To discretize equations (11) and (12), we use finite difference schemes. In order to restrict the maximum displacement change per time step from being large, equation (11) is discretized using explicit scheme with adaptive time-stepping at every point  $(i, j, k)$

$$\begin{aligned} \frac{u_1^{n+1} - u_1^n}{\Delta t} &= -[\partial_{u_1}F(\mathbf{u}^n)] - \beta(D^{x_1}v_{11}^n + D^{x_2}v_{12}^n + D^{x_3}v_{13}^n) + \beta(D^{x_1x_1}u_1^n + D^{x_2x_2}u_1^n + D^{x_3x_3}u_1^n), \\ \frac{u_2^{n+1} - u_2^n}{\Delta t} &= -[\partial_{u_2}F(\mathbf{u}^n)] - \beta(D^{x_1}v_{21}^n + D^{x_2}v_{22}^n + D^{x_3}v_{23}^n) + \beta(D^{x_1x_1}u_2^n + D^{x_2x_2}u_2^n + D^{x_3x_3}u_2^n), \\ \frac{u_3^{n+1} - u_3^n}{\Delta t} &= -[\partial_{u_3}F(\mathbf{u}^n)] - \beta(D^{x_1}v_{31}^n + D^{x_2}v_{32}^n + D^{x_3}v_{33}^n) + \beta(D^{x_1x_1}u_3^n + D^{x_2x_2}u_3^n + D^{x_3x_3}u_3^n), \end{aligned}$$

where  $[\partial_{u_l}F(\mathbf{u}^n)]$ ,  $l = 1, 2, 3$ , is a discretization of a similarity-based gradient. In our numerical experiments,  $\Delta x_1 = \Delta x_2 = \Delta x_3 = 1$ , and  $\Delta t$  is chosen so that the maximum displacement per iteration equals 0.1.

Equation (12) is discretized using semi-implicit scheme

$$\begin{aligned} \frac{v_{11}^{n+1} - v_{11}^n}{\Delta t} &= \beta(D^{x_1}u_1^n - v_{11}^{n+1}) - \nu c_1(1 + v_{11}^n) - \mu(c_2(1 + v_{11}^n) + c_5v_{12}^n + c_6v_{13}^n) \\ &\quad + \lambda((1 - v_{22}^n)(1 - v_{33}^n) - v_{32}^nv_{23}^n)L'(J), \\ \frac{v_{12}^{n+1} - v_{12}^n}{\Delta t} &= \beta(D^{x_2}u_1^n - v_{12}^{n+1}) - \nu c_1v_{12}^n - \mu(c_3v_{12}^n + c_5(1 + v_{11}^n) + c_7v_{13}^n) + \lambda(v_{23}^nv_{31}^n + v_{21}^n(1 - v_{33}^n))L'(J), \\ \frac{v_{13}^{n+1} - v_{13}^n}{\Delta t} &= \beta(D^{x_3}u_1^n - v_{13}^{n+1}) - \nu c_1v_{13}^n - \mu(c_4v_{13}^n + c_6(1 + v_{11}^n) + c_7v_{12}^n) + \lambda(v_{21}^nv_{32}^n + (1 - v_{22}^n)v_{31}^n)L'(J), \\ \frac{v_{21}^{n+1} - v_{21}^n}{\Delta t} &= \beta(D^{x_1}u_2^n - v_{21}^{n+1}) - \nu c_1v_{21}^n - \mu(c_2v_{21}^n + c_5(1 + v_{22}^n) + c_6v_{23}^n) + \lambda(v_{32}^nv_{13}^n + v_{12}^n(1 - v_{33}^n))L'(J), \\ \frac{v_{22}^{n+1} - v_{22}^n}{\Delta t} &= \beta(D^{x_2}u_2^n - v_{22}^{n+1}) - \nu c_1(1 + v_{22}^n) - \mu(c_3(1 + v_{22}^n) + c_5v_{21}^n + c_7v_{23}^n) \\ &\quad + \lambda((1 - v_{11}^n)(1 - v_{33}^n) - v_{13}^nv_{31}^n)L'(J), \\ \frac{v_{23}^{n+1} - v_{23}^n}{\Delta t} &= \beta(D^{x_3}u_2^n - v_{23}^{n+1}) - \nu c_1v_{23}^n - \mu(c_4v_{23}^n + c_6v_{21}^n + c_7(1 + v_{22}^n)) + \lambda(v_{12}^nv_{31}^n + v_{32}^n(1 - v_{11}^n))L'(J), \\ \frac{v_{31}^{n+1} - v_{31}^n}{\Delta t} &= \beta(D^{x_1}u_3^n - v_{31}^{n+1}) - \nu c_1v_{31}^n - \mu(c_2v_{31}^n + c_5v_{32}^n + c_6(1 + v_{33}^n)) + \lambda(v_{12}^nv_{23}^n + v_{13}^n(1 - v_{22}^n))L'(J), \\ \frac{v_{32}^{n+1} - v_{32}^n}{\Delta t} &= \beta(D^{x_2}u_3^n - v_{32}^{n+1}) - \nu c_1v_{32}^n - \mu(c_3v_{32}^n + c_5v_{31}^n + c_7(1 + v_{33}^n)) + \lambda(v_{21}^nv_{13}^n + v_{23}^n(1 - v_{11}^n))L'(J), \\ \frac{v_{33}^{n+1} - v_{33}^n}{\Delta t} &= \beta(D^{x_3}u_3^n - v_{33}^{n+1}) - \nu c_1(1 + v_{33}^n) - \mu(c_4(1 + v_{33}^n) + c_6v_{31}^n + c_7v_{32}^n) \\ &\quad + \lambda((1 - v_{11}^n)(1 - v_{22}^n) - v_{12}^nv_{21}^n)L'(J), \end{aligned}$$

where  $L'(J)$  is defined as in Section 3.1.

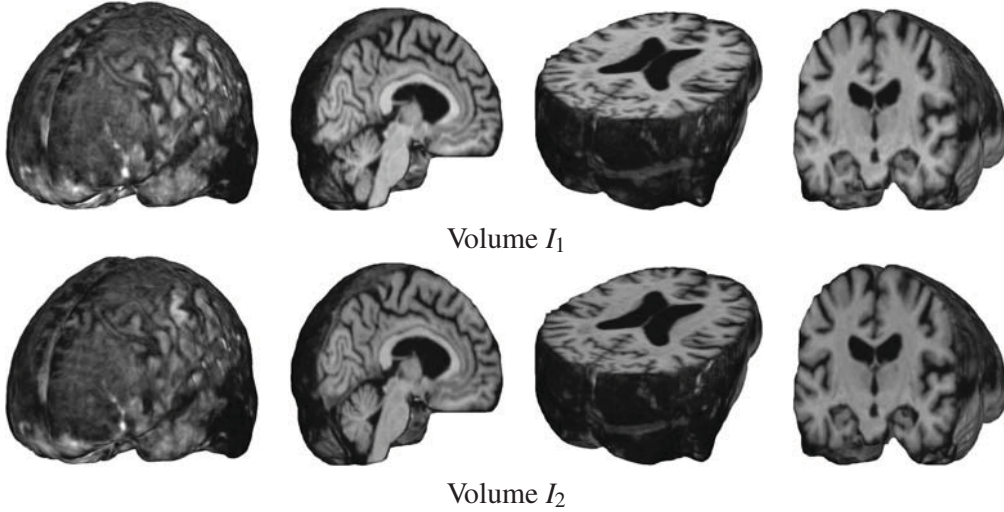


Figure 1: Serial MRI images from the ADNI follow-up dataset (images acquired one year apart) are shown. Volumes  $I_1$  (row 1) and  $I_2$  (row 2) are depicted as a brain volume (column 1) and from sagittal (column 2), axial (column 3), and coronal (column 4) views. Nonrigid registration aligns volume  $I_2$  into correspondence with volume  $I_1$ .

### 3.3 Algorithm

We are now ready to give the algorithm for the unbiased registration via nonlinear elastic regularization.

---

#### Algorithm 1 Unbiased Registration via Nonlinear Elastic Regularization

---

- 1: Initialize  $t = 0$ ,  $\mathbf{u}(\mathbf{x}, 0) = 0$ , and  $V(\mathbf{x}, 0) = 0$ .
  - 2: Calculate  $V(\mathbf{x}, t)$  using equation (12), where the equation is discretized using the semi-implicit method described in Section 3.2.  
Steps 3-5 describe the procedure for solving equation (11) advancing  $\mathbf{u}(\mathbf{x}, t)$  in time using the explicit scheme. Numerical discretization is described in Section 3.2.
  - 3: Calculate the perturbation of the displacement field  $\mathbf{R}(\mathbf{x}) = -\partial E_{\mathbf{u}}(\mathbf{u}, V)$ .
  - 4: Time step  $\Delta t$  is calculated adaptively so that  $\Delta t \cdot \max(\|\mathbf{R}\|_2) = \delta u$ , where  $\delta u$  is the maximal displacement allowed in one iteration. Results in this work are obtained with  $\delta u = 0.1$ .
  - 5: Advance equation (11), i.e.  $\partial \mathbf{u}(\mathbf{x}, t) / \partial t = \mathbf{R}(\mathbf{x})$ , in time, with time step from step 4, solving for  $\mathbf{u}(\mathbf{x}, t)$ .
  - 6: If the cost functional in (10) decreases by sufficiently small amount compared to the previous iteration, then stop.
  - 7: Let  $t := t + \Delta t$  and go to step 2.
- 

## 4 Results and Discussion

We tested the proposed *unbiased nonlinear elastic* registration model and compared the results to those obtained with the *unbiased fluid registration* method [16], where the unbiased regularization constraint (8) was coupled with the  $L^2$  matching functional (3) and fluid regularization (1), (2). Here, both methods were coupled with the  $L^2$  and mutual information (MI) based similarity measures. In our experiments, we used a pair of serial MRI images ( $220 \times 220 \times 220$ ) from the Alzheimer's Disease Neuroimaging Initiative (ADNI). Since the images were acquired one year apart, from a subject with Alzheimer's disease, real anatomical changes are present, which allows methods to be compared in the presence of true biological changes.

In the tests performed using unbiased nonlinear elasticity coupled with  $L^2$  matching, values of  $\beta = 20000$



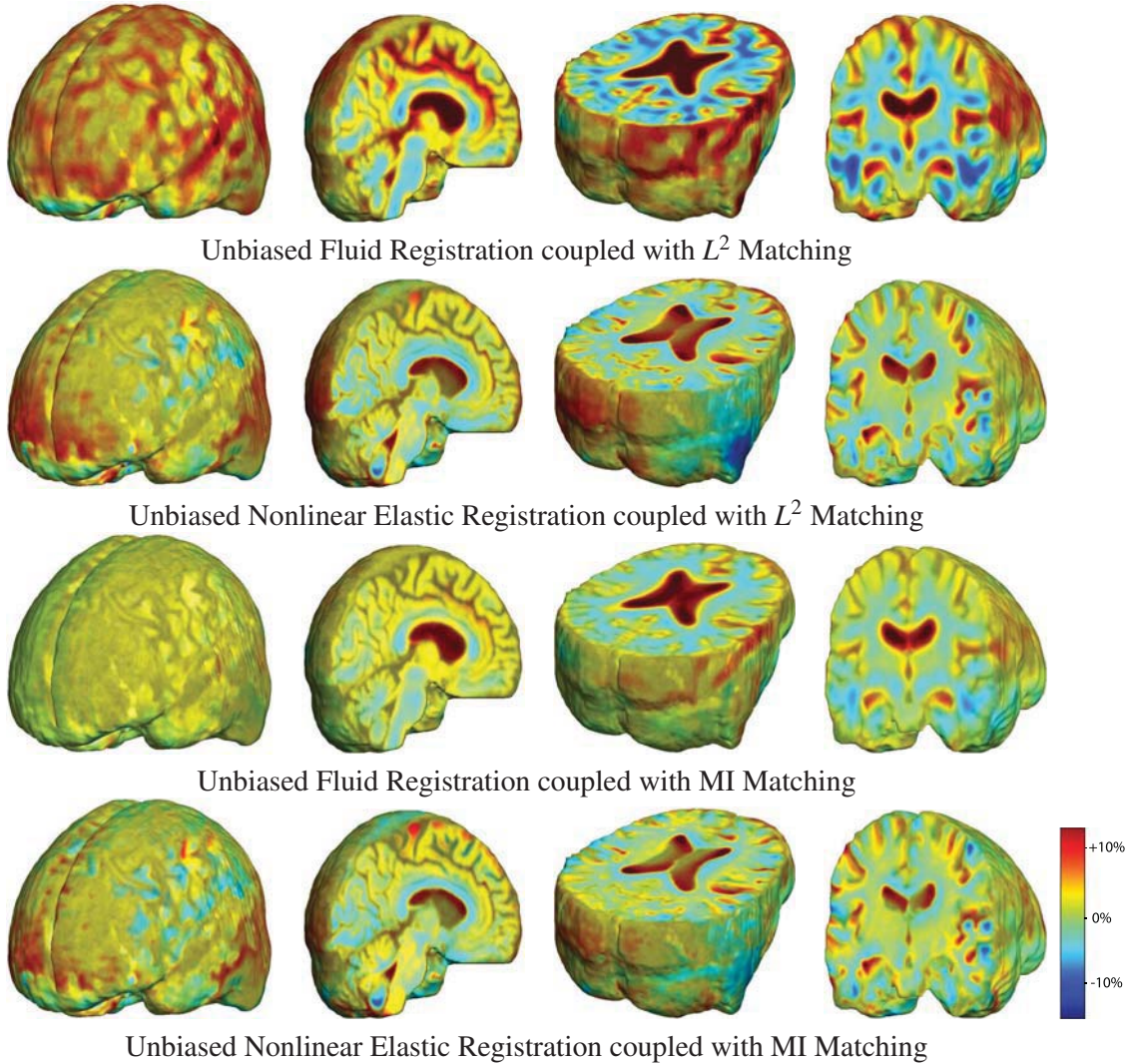


Figure 2: Nonrigid registration was performed on the Serial MRI images from the ADNI Follow-up dataset using unbiased fluid registration and unbiased nonlinear elasticity registration, both coupled with  $L^2$  and MI matching. Jacobian maps are superimposed on the target volume.

in equation (7) and  $\lambda = 2000$  in equation (10) were chosen. For MI matching,  $\beta = 80$  and  $\lambda = 8$  were used. The values of the Lamé coefficients were chosen to be equal,  $\mu = \nu$ , in all experiments. Bigger values of  $\mu$  and  $\nu$  allow for more smoothing. For unbiased fluid registration model, described in [16],  $\lambda = 500$  was chosen for  $L^2$  matching, and  $\lambda = 5$  for MI matching.

Figure 1 shows the images being registered and Figures 2 shows the resulting Jacobian maps. Results generated using the fluid and nonlinear elasticity based unbiased models are similar, both suggesting a mild volume reduction in gray and white matter and ventricular enlargement that is observed in Alzheimer's disease patients. The advantages of the unbiased nonlinear elasticity model is its more locally plausible reproduction of atrophic changes in the brain and its robustness to original misalignment of brain volumes, which is especially noticeable on the brain surface. The unbiased nonlinear elasticity model coupled with  $L^2$  matching generated very similar results to those obtained with the MI similarity measure, partly because difference images typically contain only noise after registration. Unbiased fluid registration method, however, is more effective in modeling the regional neuroanatomical changes, showing more clearly which parts

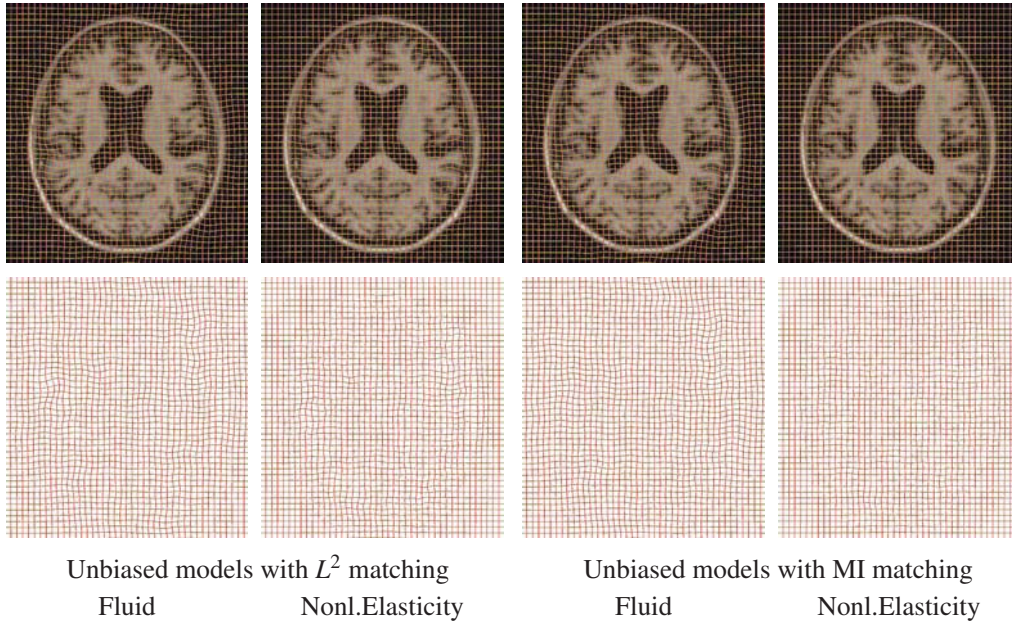


Figure 3: Results obtained using unbiased fluid registration and unbiased nonlinear elasticity registration, both coupled with  $L^2$  and MI matching. The generated grids are superimposed on top of 2D cross-sections of the 3D volumes (row 1) and are shown separately (row 2).

of the volume have undergone largest tissue changes, such as ventricular enlargement as shown in Figure 2.

Figure 3 shows deformed grids generated with unbiased fluid and unbiased nonlinear elastic registration models. Figure 4 shows the energy decrease per iteration for both models. Note that the unbiased fluid registration minimizes the energy defined as  $E(\mathbf{u}) = F(\mathbf{u}) + \lambda R_{UB}(\mathbf{u})$ .

In Figure 5, we examined the *inverse consistency* of the mappings [4] generated using unbiased nonlinear elastic registration. Here, the deformation was computed in both directions (time 2 to time 1, and time 1 to time 2) using MI matching. The forward and backward Jacobian maps were concatenated (in an ideal situation, this operation should yield the identity), with the products of Jacobians having values close to 1.

The unbiased nonlinear elasticity model does not require expensive Navier-Stokes solver (or its approximation), which is employed at each iteration for fluid flow models. Hence, unbiased nonlinear elasticity model is more efficient than the unbiased fluid step. In our future studies, we will examine the registration accuracy of the different models where ground truth is known, and will compare each model’s power for detecting inter-group differences or statistical effects on rates of atrophy.

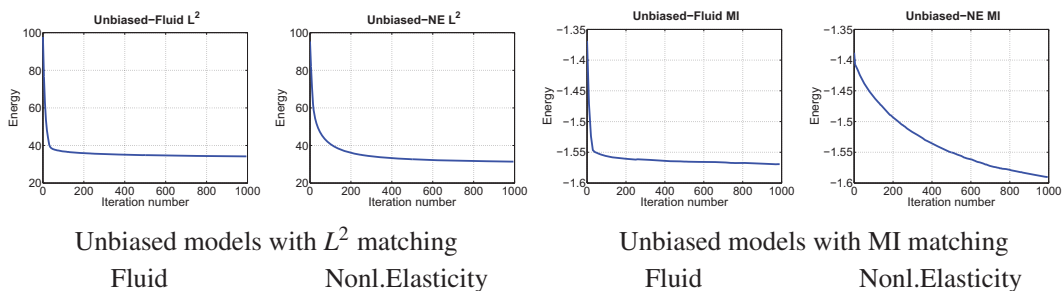


Figure 4: Energy per iteration for the unbiased fluid registration and unbiased nonlinear elasticity registration, both coupled with  $L^2$  and MI matching.



## Acknowledgements

This work was funded by the National Institutes of Health through the NIH Roadmap for Medical Research, Grant U54 RR021813.

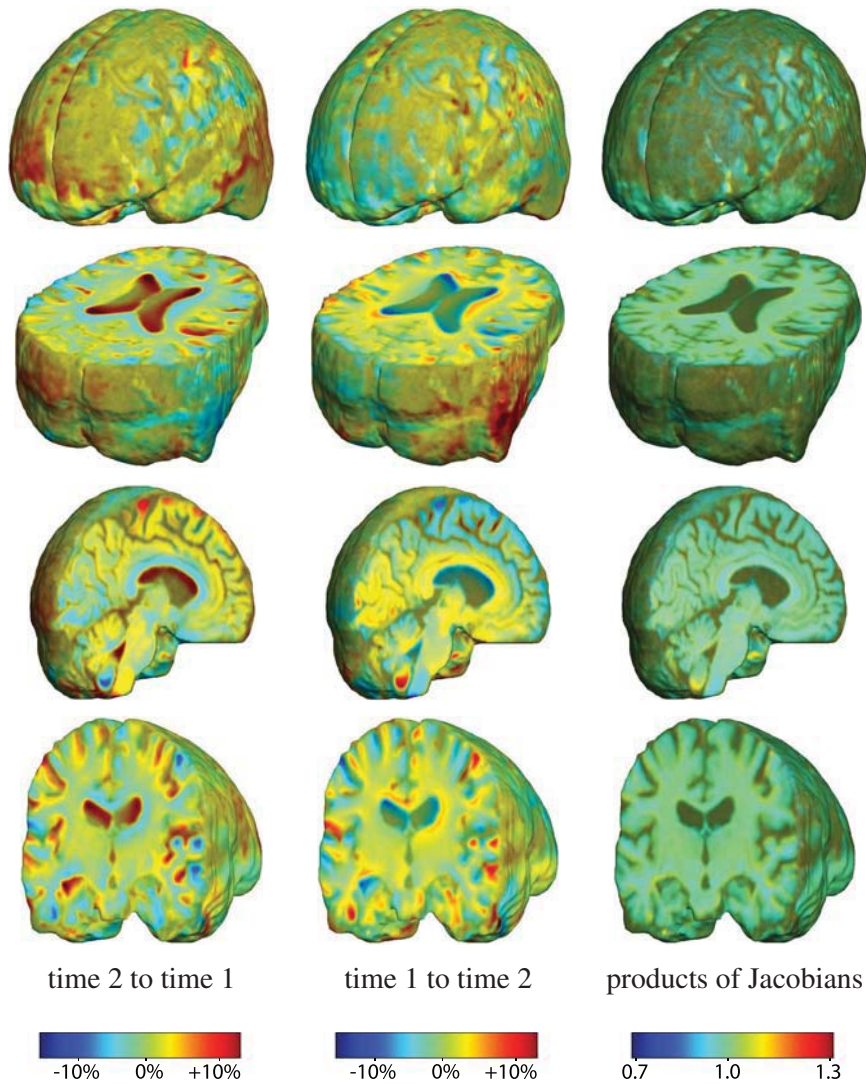


Figure 5: This figure examines the inverse consistency of the unbiased nonlinear elastic registration. Here, the model is coupled with mutual information matching. Jacobian maps of deformations from time 2 to time 1 (column 1) and time 1 to time 2 (column 2) are superimposed on the target volumes. The products of Jacobian maps, shown in column 3, have values close to 1, suggesting inverse consistency.

## References

- [1] M. Bro-Nielsen and C. Gramkow. Fast fluid registration of medical images. In *Visualization in Biomedical Computing*, pages 267–276, 1996.
- [2] C. Broit. *Optimal Registration of Deformed Images*. PhD thesis, University of Pennsylvania, 1981.



- [3] C. Brun, N. Lepore, X. Pennec, Y. Chou, O. Lopez, H. Aizenstein, J. Becker, A. Toga, and P. Thompson. Comparison of standard and Riemannian elasticity for tensor-based morphometry in HIV/AIDS. *International Conference on Medical Image Computing and Computer Assisted Intervention*, 2007.
- [4] G. Christensen and H. Johnson. Consistent image registration. *IEEE Transactions on Medical Imaging*, 20(7):568–582, 2001.
- [5] G. Christensen, R. Rabbitt, and M. Miller. Deformable templates using large deformation kinematics. *IEEE Transactions on Image Processing*, 5(10):1435–1447, 1996.
- [6] A. Collignon, F. Maes, D. Delaere, D. Vandermeulen, P. Suetens, and G. Marchal. Automated multi-modality image registration based on information theory. In Y. Bizais, C. Barillot, and R. Di Paola, editors, *Information Processing in Medical Imaging*, volume 3, pages 264–274. Kluwer Academic Publishers, Dordrecht, 1995.
- [7] E. D’Agostino, F. Maes, D. Vandermeulen, and P. Suetens. A viscous fluid model for multimodal non-rigid image registration using mutual information. *Medical Image Analysis*, 7:565–575, 2003.
- [8] E. Haber and J. Modersitzki. Numerical methods for volume preserving image registration. *Inverse problems*, Institute of Physics Publishing, 20(5):1621–1638, 2004.
- [9] E. Haber and J. Modersitzki. Image registration with guaranteed displacement regularity. *International Journal of Computer Vision*, 71(3):361–372, 2007.
- [10] N. Lord, J. Ho, B. Vemuri, and S. Eisenschenk. Simultaneous registration and parcellation of bilateral hippocampal surface pairs for local asymmetry quantification. *IEEE Transactions on Medical Imaging*, 26(4):471–478, 2007.
- [11] J. Modersitzki. *Numerical Methods for Image Registration (Numerical Mathematics and Scientific Computation)*. Oxford University Press, New York, 2004.
- [12] P. Negron-Marrero. A numerical method for detecting singular minimizers of multidimensional problems in nonlinear elasticity. *Numerische Mathematik*, 58(1):135–144, 1990.
- [13] X. Pennec. Left-invariant riemannian elasticity: A distance on shape diffeomorphisms? *International Workshop on Mathematical Foundations of Computational Anatomy*, pages 1–13, 2006.
- [14] X. Pennec, R. Stefanescu, V. Arsigny, P. Fillard, and N. Ayache. Riemannian elasticity: A statistical regularization framework for non-linear registration. In *International Conference on Medical Image Computing and Computer Assisted Intervention*, pages 943–950, 2005.
- [15] P. Viola and W. Wells. Alignment by maximization of mutual information. *International Conference on Computer Vision*, pages 16–23, 1995.
- [16] Igor Yanovsky, Paul Thompson, Stanley Osher, and Alex Leow. Topology preserving log-unbiased nonlinear image registration: Theory and implementation. *IEEE Conference on Computer Vision and Pattern Recognition*, pages 1–8, 2007.
- [17] Igor Yanovsky, Paul Thompson, Stanley Osher, and Alex Leow. Asymmetric and symmetric unbiased image registration: Statistical assessment of performance. *IEEE Computer Society Workshop on Mathematical Methods in Biomedical Image Analysis*, 2008.